Iterative approach to arbitrary nonlinear optical response functions of graphene

F. Hipolito,[1,*] Darko Dimitrovski,[1] and T. G. Pedersen[1,2,†]
[1]*Department of Physics and Nanotechnology, Aalborg University, DK-9220 AalborgØst, Denmark*
[2]*Center for Nanostructured Graphene (CNG), DK-9220 AalborgØst, Denmark*

(Received 15 January 2019; revised manuscript received 12 April 2019; published 6 May 2019)

Two-dimensional materials constitute an exciting platform for nonlinear optics with large nonlinearities that are tunable by gating. Hence, gate-tunable harmonic generation and intensity-dependent refraction have been observed in, e.g., graphene and transition-metal dichalcogenides, whose electronic structures are accurately modeled by the (massive) Dirac equation. We exploit on the simplicity of this model and demonstrate here that arbitrary nonlinear response functions follow from a simple iterative approach. The power of this approach is illustrated by analytical expressions for harmonic generation and intensity-dependent refraction, both computed up to ninth order in the pump field. Moreover, the results allow for arbitrary band gaps and gating potentials. As illustrative applications, we consider (i) the gate dependence of third- and fifth-harmonic generation in gapped and gapless graphene, (ii) the intensity-dependent refractive index of graphene up to ninth order, and (iii) the intensity dependence of high-harmonic generation.

DOI: 10.1103/PhysRevB.99.195407

The nonlinear optical (NLO) response encompasses a large class of light matter interactions [1–6], including processes such as harmonic generation and self-focusing of light, that has proven useful in a number of applications in nonlinear spectroscopy and in optoelectronic devices. Recent progress in the fabrication of two-dimensional (2D) materials has produced a new fertile class of materials with large nonlinear susceptibilities [7]. Recent reports include measurements of high-harmonic generation (HHG) [8,9] and intensity-dependent refractive index [10,11] in graphene and in transition-metal dichalcogenides (TMDs) [12]. In addition, it has been shown that the NLO response can be tuned by electrostatic doping [13–15] and significant progress has been made in measuring the even-order NLO response in TMDs [16,17]. Furthermore, the nonlinearities in 2D materials can be significantly enhanced by several mechanisms such as plasmons [18–20], polaritonic effects [21], and metasurfaces [22].

Compared with the linear response, calculations of NLO processes in crystals are significantly more complex. Whereas the linear response results from purely inter- or intraband processes, the NLO response contains not only these processes, but also mixed ones involving both the inter- and intraband motion of electrons [23–26]. To circumvent this complexity, the NLO response has been characterized using several theoretical methods, each with its own merits and shortcomings: (i) a perturbative expansion of the reduced density matrix [26–28]; (ii) time-dependent techniques [29–32]; and (iii) the Wannier representation [33]. The perturbative method offers a feasible approach to specific processes at a fixed frequency and power of the external field. The standard approach expands all matrix elements in unperturbed eigenstates, leading to increasingly complicated sum-over-states expressions for high-order processes. Still, within the perturbative regime, highly accurate results are obtained and in simple few-band systems such as the Dirac Hamiltonian, closed-form solutions can often be found. These allow for characterization with respect to external parameters, for instance, doping and temperature [26–28]. Yet, the growth in complexity associated with mixed inter- and intraband motion makes calculations extremely cumbersome beyond third order. The complicated nature of the general third-order response [26] testifies to this complexity. Methods (ii) and (iii) can be applied to study the NLO response at field strengths beyond the perturbative regime, as these intrinsically include contributions from all powers of the external field. But, in contrast to perturbative approaches, these methods rely extensively on numerical techniques for the integration of the equation of motion and for the Fourier transforms required to analyze the response in the frequency domain, thus making the characterization of the NLO response with respect to external parameters an elaborate numerical process [29–32].

In the present paper, we study the (massive and massless) Dirac Hamiltonian as a model of graphene and TMDs. For this important class of materials, we bridge a key shortcoming found in perturbative techniques by evaluating the current density response via an iterative solution. This approach allows for the evaluation of arbitrarily high-order response functions. As an illustration, we compute all response functions up to ninth order for (gapped) graphene [34]. The massive Dirac Hamiltonian [35] with a external vector potential $\mathbf{A} = \mathbf{A}_0 \sin(\omega t)$ reads, using the minimal coupling (velocity gauge) [36],

$$H = v_F(\hbar\boldsymbol{\kappa} + e\mathbf{A}) \cdot \boldsymbol{\sigma} + \hbar\Delta\sigma_z, \tag{1}$$

where $v_F \sim 10^6$ m/s is the Fermi velocity, $\boldsymbol{\kappa}$ is the wave vector, $\boldsymbol{\sigma}$ are the Pauli matrices, $\Delta \geqslant 0$ is the mass term, and $e > 0$. This model leads to a gapped band structure with

*fh@nano.aau.dk
†tgp@nano.aau.dk

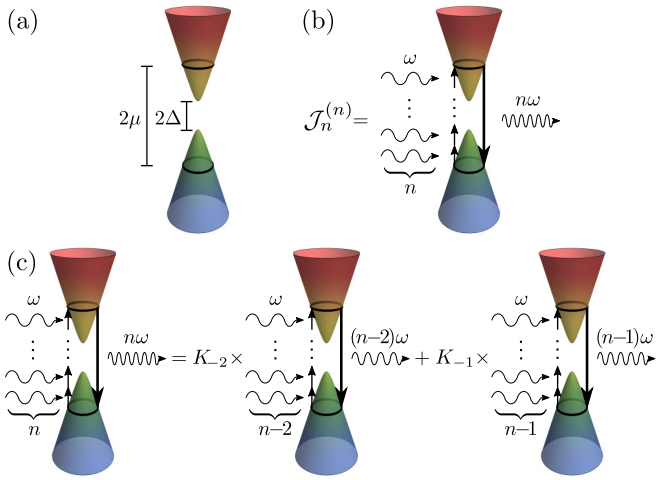

FIG. 1. Diagrammatic representation of the band structure (a) of the nth-harmonic integrand $\mathcal{J}_n^{(n)}$ at the resonance $2\mu = n\omega$ and (b) of the iterative solution for $\mathcal{J}_n^{(n)}$ integrand (for nth harmonic) as in Eq. (7). Here, $\mathcal{J}_n^{(n)}$ represents absorption of n photons with frequency ω, followed by the emission of a single photon with frequency $n\omega$.

energy gap $E_g = 2\hbar\Delta$, and doping is including via a nonvanishing Fermi level $\hbar\mu$. Hence, for pristine graphene, we take $\Delta = 0$. The key features of the electronic structure are shown in Fig. 1(a). The Dirac Hamiltonian has proven extremely useful for systems with threefold rotation symmetry. It allows for an accurate analytic characterization of several physical properties in graphene [37] and in the vast class of TMDs [38].

The time evolution of the wave function ψ governed by $i\hbar\dot{\psi} = H\psi$ is found by expanding in the eigenstates $u_{1,2}$ of the unperturbed Hamiltonian, i.e., taking $\mathbf{A} = \mathbf{0}$. We write the general wave function as

$$\psi = [a(t)u_1 + b(t)u_2]\exp[i(\boldsymbol{\kappa}\cdot\mathbf{r} + \epsilon t)], \tag{2}$$

with energy dispersion $\epsilon = \sqrt{\Delta^2 + k^2}$ (in frequency units), and $k = v_F|\boldsymbol{\kappa}|$. Furthermore, we focus on the response to a normally incident, linearly polarized monochromatic field $\mathbf{A} = A\mathbf{e}_x$ and define $\mathcal{A}(t) = v_F eA_0\sin(\omega t)/\hbar = \mathcal{A}_0\sin(\omega t)$, which is related to the electric field $\mathcal{E}(t) = \mathcal{E}_0\cos(\omega t)$ by $\mathcal{E}_0 = -\omega A_0$. The time evolution of the coefficients follows from $\dot{a}(t) = i\mathcal{A}(t)[a(t)F - b(t)G]$ and $i\dot{b}(t) = \mathcal{A}(t)G^*a(t) + [2\epsilon + \mathcal{A}(t)F]b(t)$, where $F = \sqrt{\epsilon^2 - \Delta^2}\cos(\theta)/\epsilon$ and $G = [\Delta\cos(\theta) - i\epsilon\sin(\theta)]/\epsilon$ arise from matrix elements of the velocity operator. The coefficients then determine the reduced density matrix, whose matrix elements read $\rho_{11} = |a|^2$, $\rho_{22} = |b|^2$, and $\rho_{21} = a^*b$. In turn, their time evolution is governed by

$$i\dot{\mathcal{N}} = -2\mathcal{A}(t)(\mathcal{P}G - G^*\mathcal{P}^*), \tag{3a}$$

$$i\dot{\mathcal{P}} = -\mathcal{A}(t)G^*\mathcal{N} + 2[\mathcal{A}(t)F + \epsilon]\mathcal{P}, \tag{3b}$$

where $\mathcal{N} = \rho_{22} - \rho_{11}$ and $\mathcal{P} = \rho_{21}$ define the population difference and coherence, respectively. Finally, the current density is evaluated via the expectation value of the current density operator $j = -eg_sg_v(2\pi)^{-2}v_F\int\mathcal{J}d\boldsymbol{\kappa}$, where the dimensionless integrand for the current density response is defined by $\mathcal{J} = \sum_{mn}v_{nm}\rho_{mn}/v_F = F\mathcal{N} + \mathcal{P}G + G^*\mathcal{P}^*$ using the matrix elements v_{nm} of the velocity operator $\hat{v}_x = v_F\hat{\sigma}_x$. Here, $g_s = 2$ and $g_v = 2$ are spin and valley degeneracies, respectively.

The iterative sequence is found by considering the first- and second-order time derivatives of $\mathcal{J}$ that read

$$\mathcal{A}(t)\dot{\mathcal{J}} = -\epsilon\ddot{\mathcal{N}}, \tag{4a}$$

$$\ddot{\mathcal{J}} = 4\epsilon[\mathcal{A}(t) + \epsilon F]\mathcal{N} - 4\epsilon[\mathcal{A}(t)F + \epsilon]\mathcal{J}. \tag{4b}$$

Using a time-harmonic expansion for the integrand $\mathcal{J} = \sum_n\mathcal{J}_ne^{-in\omega t}$ and for the population $\mathcal{N} = \sum_n\mathcal{N}_ne^{-in\omega t}$, the dynamical equations can be cast as

$$\mathcal{A}_0[(n-1)\mathcal{J}_{n-1} - (n+1)\mathcal{J}_{n+1}] = 2in\epsilon\mathcal{N}_n, \tag{5a}$$

$$(4\epsilon^2 - n^2\omega^2)\mathcal{J}_n = 4\epsilon^2F\mathcal{N}_n - 2i\epsilon\mathcal{A}_0F(\mathcal{J}_{n-1} - \mathcal{J}_{n+1}) + 2i\epsilon\mathcal{A}_0(\mathcal{N}_{n-1} - \mathcal{N}_{n+1}), \tag{5b}$$

where $n \in \mathbb{Z}$ defines the Fourier order. The final iterative series for the integrand is identified by making use of an expansion with respect to powers of the external field $\mathcal{J}_n = \sum_{j\geqslant n}\mathcal{J}_n^{(j)}\mathcal{A}_0^j$ and collecting equal powers [39]

$$\begin{aligned}\mathcal{J}_n^{(j)} &= \Theta_{j,n+4}K_2\mathcal{J}_{n+2}^{(j-2)} \\ &+ \Theta_{j,n+2}\big[\Theta_{j,2}\bar{\delta}_{n,1}K_0\mathcal{J}_n^{(j-2)} + \bar{\delta}_{n,0}K_1\mathcal{J}_{n+1}^{(j-1)}\big] \\ &+ \Theta_{j,n}\big[\Theta_{j,2}K_{-2}\mathcal{J}_{n-2}^{(j-2)} + \bar{\delta}_{n,0}K_{-1}\mathcal{J}_{n-1}^{(j-1)}\big],\end{aligned} \tag{6}$$

where $n + j \geqslant 1$, $\Theta_{i,j}$ is the discrete unit step function [40], $\bar{\delta}_{i,j} \equiv 1 - \delta_{i,j}$, and the coefficients read $K_0 = 2n^2/[Q_n(n^2-1)]$, $K_{\pm1} = \mp 2iF\epsilon(2n\pm1)/(Q_nn)$, and $K_{\pm2} = -(n\pm2)/[Q_n(n\pm1)]$ with $Q_n = 4\epsilon^2 - n^2\omega^2$. The dominant term in harmonic generation emerges from the diagonal case $j = n > 2$, where the general solution Eq. (6) reduces to

$$\mathcal{J}_n^{(n)} = K_{-2}\mathcal{J}_{n-2}^{(n-2)} + K_{-1}\mathcal{J}_{n-1}^{(n-1)}, \tag{7}$$

which lends itself to a diagrammatic representation as illustrated in Figs. 1(b) and 1(c).

To apply the iterative solution for $\mathcal{J}_n^{(j)}$ in practice, two seeds $\mathcal{J}_0^{(0)}$ and $\mathcal{J}_1^{(1)}$ are required that can easily be determined from low-order terms in Eq. (5b). Collecting all terms independent of the external field and making use of the equilibrium charge distribution $\mathcal{N}_0 = f_1 - f_2$ (the difference between Fermi functions), the first seed reads $\mathcal{J}_0^{(0)} = F\mathcal{N}_0$. The second seed involves the collection of linear terms in the external field and reads $\mathcal{J}_1^{(1)} = 2i\epsilon|G|^2\mathcal{N}_0\mathcal{A}_0/[4\epsilon^2 - \omega^2]$. All remaining terms of $\mathcal{J}_n^{(j)}$ can be computed sequentially by evaluating all possible Fourier components $n = \{0, 1, \ldots, j\}$, in increasing order, for any given response order j using Eq. (6). The solutions for all nonzero integrands up to fifth order are listed in this order in Table I. The final response functions are obtained by integrating the desired $\mathcal{J}_n^{(j)}$ over κ space and the respective conductivities $\sigma_n^{(j)}(\omega)$ then follow by writing

$$j(t) = \sum_{n,j}\big[\sigma_n^{(j)}(\omega)\mathcal{E}_0^je^{-in\omega t} + \text{c.c.}\big]/2. \tag{8}$$

TABLE I. Analytic expressions for current density integrands up to fifth order, where $\mathcal{J}_n^{(j)} \equiv \mathcal{F}_n^{(j)}|G|^2\mathcal{N}_0\mathcal{A}_0^j$.

(n, j)	$\mathcal{F}_n^{(j)}$
(0,0)	$F/\|G\|^2$
(1,1)	$2i\epsilon/[4\epsilon^2-\omega^2]$
(0,2)	$-2F/[4\epsilon^2-\omega^2]$
(2,2)	$6\epsilon^2F/[(4\epsilon^2-4\omega^2)(4\epsilon^2-\omega^2)]$
(1,3)	$4i\epsilon[(13F^2-1)\epsilon^2-(4F^2-1)\omega^2]/[(4\epsilon^2-4\omega^2)(4\epsilon^2-\omega^2)^2]$
(3,3)	$-4i\epsilon[(5F^2-1)\epsilon^2+\omega^2]/[(4\epsilon^2-9\omega^2)(4\epsilon^2-4\omega^2)(4\epsilon^2-\omega^2)]$
(0,4)	$-2F[2(13F^2-7)\epsilon^2-(8F^2-5)\omega^2]/[(4\epsilon^2-4\omega^2)(4\epsilon^2-\omega^2)^2]$
(2,4)	$16\epsilon^2F[8(8F^2-3)\epsilon^4-2(53F^2-28)\epsilon^2\omega^2+(27F^2-17)\omega^4]/[(4\epsilon^2-9\omega^2)(4\epsilon^2-4\omega^2)^2(4\epsilon^2-\omega^2)^2]$
(4,4)	$-10\epsilon^2F[(7F^2-3)\epsilon^2+5\omega^2]/[8(4\epsilon^2-16\omega^2)(4\epsilon^2-9\omega^2)(4\epsilon^2-4\omega^2)(4\epsilon^2-\omega^2)]$
(1,5)	$48i\epsilon[8(61F^4-32F^2+1)\epsilon^6-2(503F^4-334F^2+11)\epsilon^4\omega^2+5(100F^4-77F^2+4)\epsilon^2\omega^4-3(24F^4-21F^2+2)\omega^6]/[(4\epsilon^2-9\omega^2)(4\epsilon^2-4\omega^2)^2(4\epsilon^2-\omega^2)^3]$
(3,5)	$-16i\epsilon[4(295F^4-186F^2+11)\epsilon^8-(5235F^4-4166F^2+291)\epsilon^6\omega^2+(6095F^4-6303F^2+558)\epsilon^4\omega^4-(1440F^4-2569F^2+419)\epsilon^2\omega^6+36(3-8F^2)\omega^8]/[(4\epsilon^2-16\omega^2)(4\epsilon^2-4\omega^2)^2(4\epsilon^2-9\omega^2)^2(4\epsilon^2-\omega^2)^2]$
(5,5)	$12i\epsilon[(21F^4-14F^2+1)\epsilon^4-5(1-7F^2)\epsilon^2\omega^2+4\omega^4]/[(4\epsilon^2-25\omega^2)(4\epsilon^2-16\omega^2)(4\epsilon^2-9\omega^2)(4\epsilon^2-4\omega^2)(4\epsilon^2-\omega^2)]$

In most cases, the integration is straightforward, but can lead to cumbersome expressions, particularly whenever the difference between the Fourier n and response order j is large. The angular part of the integral depends exclusively on powers of F and $|G|$, therefore it can be shown that due to the presence of full rotation symmetry in the effective Hamiltonian all even-order response functions vanish upon angular integration. Nonetheless, even-order integrands remains necessary to determine higher-order nonvanishing odd integrands.

Now, we turn our attention to the conductivities computed within the iterative framework. At low temperatures the population difference becomes a step function $\mathcal{N}_0 = -\Theta(\epsilon - |\mu|)$ and the lower limit Ω of the radial part of the integral is determined by the larger of the Fermi level and mass term, i.e., $\Omega \equiv \max(|\mu|, \Delta)$ [41]. In our explicit examples, we compute all conductivities up to ninth order [34]. Among these, we examine third- and fifth-harmonic generation (THG and FHG), as well as intensity-dependent refraction through the optical Kerr effect including high-order terms. As demonstrated in recent experiments [13–15], valuable information can be extracted by varying the Fermi level via electrostatic gating. Hence, we apply the present results to study the doping dependence of these NLO processes.

The THG conductivity reads

$$\begin{aligned}\sigma_3^{(3)}(\omega) = {}& \frac{-3i\sigma_3}{1024\pi}\left(\frac{2v_F}{3a_0\omega}\right)^4 \\ &\times\left[\left(45+\frac{56\Delta^2}{\omega^2}-\frac{48\Delta^4}{\omega^4}\right)\ln\frac{2\Omega-3\omega}{2\Omega+3\omega}\right. \\ &-\left(64+\frac{128\Delta^2}{\omega^2}-\frac{192\Delta^4}{\omega^4}\right)\ln\frac{2\Omega-2\omega}{2\Omega+2\omega} \\ &\left.+\left(17+\frac{88\Delta^2}{\omega^2}-\frac{240\Delta^4}{\omega^4}\right)\ln\frac{2\Omega-\omega}{2\Omega+\omega}\right], \end{aligned} \tag{9}$$

where we define the scale of the 2D nonlinear conductivities systematically by $\sigma_{j>1} \equiv 2[3ea_0^2/(4\hbar v_F)]^{j-1}\sigma_1$ with $\sigma_1 = e^2/(4\hbar)$ and the carbon-carbon distance $a_0 \equiv 1.42$ Å sets the natural length scale for graphene. Throughout this paper, we consider exclusively electron doping $\mu > 0$, but results for hole doping $\mu < 0$ simply follow by replacing $\mu \to -\mu$. Taking the limit $\Delta \to 0$, one can verify that our expression reduces to previous results derived with the gapless Dirac Hamiltonian using velocity and length gauges [26–28]. The expression for $\sigma_3^{(3)}(\omega)$ is representative of the HHG conductivities $\sigma_n^{(n)}(\omega)$, which are always composed of n logarithmic divergences, whose amplitude is set by a polynomial prefactor with even powers of Δ/ω, as shown in Eq. (C1a). Note that the divergences found in the expressions are regularized by introducing a small broadening parameter $\omega \to \omega + i\eta$ and, unless stated otherwise, we use $\hbar\eta = 1$ meV. The THG conductivities for both gapped and gapless graphene assuming photon energies in the low and medium range are shown in Fig. 2. Given the rather small gaps that can be reliably generated in graphene [42,43] (we take $E_g \equiv 250$ meV as a

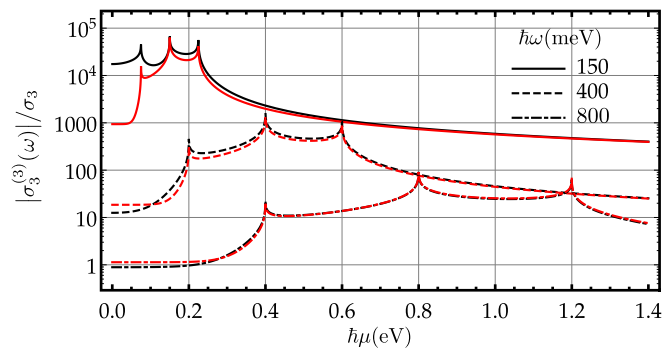

FIG. 2. THG conductivity in gapped (E_g=250 meV, black) and gapless (red) graphene at photon energies $\hbar\omega$={150, 400, 800} meV.

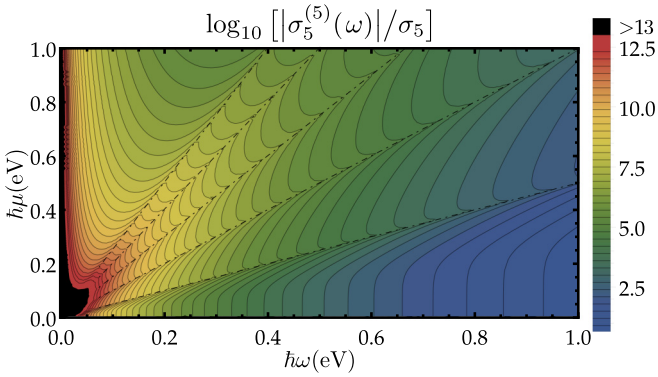

FIG. 3. Contour plot of FHG conductivity in graphene. Dotted-dashed lines show the resonant conditions $\mu = m\omega/2$, $m = \{1, 2, 3, 4, 5\}$, and the conductivity in the black region exceeds $10^{13}\sigma_5$.

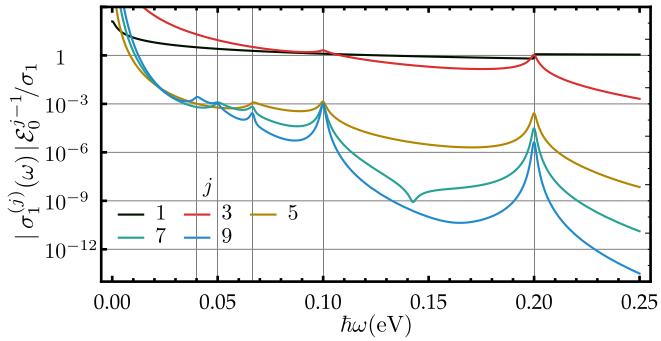

FIG. 4. Linear and nonlinear contributions to the optical conductivity in doped graphene $\hbar\mu = 100$ meV at $\mathcal{E}_0 = 2$ V/μm. The black curve is the linear response and colored lines represent the nonlinearities. Vertical grid lines represent the $(n + j)/2$ resonances found in the nonlinear conductivities.

reference figure for our calculations) and considering photon energies $\hbar\omega > 150$ meV, our results show that the response of gapless and gapped systems are generally similar but deviate whenever $\mu \lesssim \Delta$.

The FHG conductivity in gapless graphene also lends itself to a closed-form expression [34], with $n = 5$ logarithmic divergences,

$$\sigma_5^{(5)}(\omega) = \frac{9i\sigma_5}{655360\pi}\left(\frac{2v_F}{3a_0\omega}\right)^8\left[4925\ln\frac{2\mu-5\omega}{2\mu+5\omega} - 16384\ln\frac{2\mu-4\omega}{2\mu+4\omega} + 19359\ln\frac{2\mu-3\omega}{2\mu+3\omega} - 9216\ln\frac{2\mu-2\omega}{2\mu+2\omega} + 1266\ln\frac{2\mu-\omega}{2\mu+\omega}\right], \quad (10)$$

where the general expression valid for $\Delta \neq 0$ is given in Eq. (C3) [34]. The fifth-order response of graphene is highly sensitive to the ratio between photon energy and doping level. This is illustrated in the contour plot in Fig. 3 of the amplitude of the FHG conductivity as a function of these parameters. It shows that this response function can be tuned over several orders of magnitude by tuning either parameter, while highlighting the five resonances present in the FHG response. Moreover, we find that the nonlinear conductivities of graphene are regular in the limit of vanishing doping $\mu \to 0$,

$$\lim_{\mu\to 0}\sigma_n^{(j)}/\sigma_j = q_{nj}[2v_F/(3a_0\omega)]^{2(j-1)}, \quad (11)$$

where the coefficients q_{nj} are rational numbers. The complete list for all coefficients is found in Table II in Appendix C. For THG and FHG, the coefficients read $q_{33} = 3/512$ and $q_{55} = -45/65536$, respectively.

The iterative approach can also readily be used to evaluate conductivities beyond harmonic generation such as the optical Kerr conductivity of graphene [34],

$$\sigma_1^{(3)}(\omega) = \frac{9i\sigma_3}{256\pi}\left(\frac{2v_F}{3a_0\omega}\right)^4\left[\frac{12\mu\omega}{4\mu^2-\omega^2} - 11\ln\frac{\omega-2\mu}{\omega+2\mu} + 16\ln\frac{2\omega-2\mu}{2\omega+2\mu}\right]. \quad (12)$$

This expression is representative of high-order contributions to any Fourier order $\sigma_n^{(j>n)}$ [34]. These expressions contain $(j + n)/2$ logarithmic divergences, rather than $j = n$ found in the nth-harmonic conductivities, and also contain an additional rational function with $(j + n - 2)/2$ polynomial divergences that strongly enhance the nonlinear resonances (see Fig. 6 in Appendix A). In Fig. 4, we show the conductivities $\sigma_1^{(j)}$ contributing to the first harmonic current in doped graphene up to ninth order at $\mathcal{E}_0 = 2$ V/μm. Note that the field intensity considered in Fig. 4 matches the upper limit of the perturbative regime when considering THz radiation [9]. Inspection of Fig. 4 defines the regime where the perturbative approach breaks down, namely, the frequency range, in which terms $\sigma_1^{(j)}\mathcal{E}_0^{j-1}$ cease to decrease as the order j is increased. Hence, for the parameters in Fig. 4, the nonperturbative region can be estimated as $\hbar\omega \lesssim 60$ meV. Manifestations from higher than Kerr terms should be detectable as higher-order terms introduce additional resonances that are highly sensitive to both the Fermi level and the magnitude of the external field.

In Fig. 5, we plot the relative amplitude of the Fourier components of the radiated intensity $I_n(\omega) = \mu_0 c|j_n(\omega)|^2/8$ with

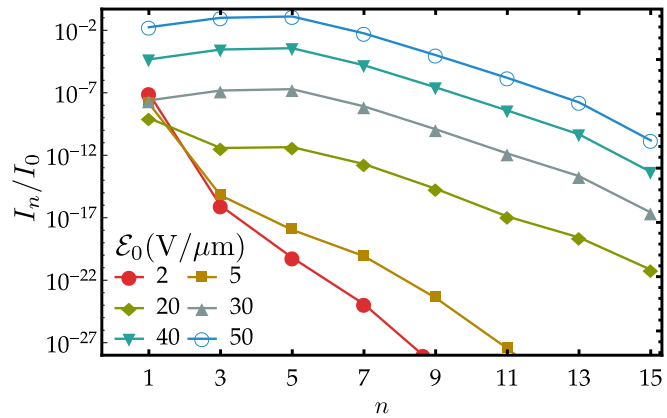

FIG. 5. Intensity of HHG Fourier components in doped graphene ($\hbar\mu = 250$ meV) normalized by $I_0 = \varepsilon_0 c_0 \mathcal{E}_0^2/2$. The incident photon energy is $\hbar\omega = 100$ meV and colors red to blue represent increasing field strengths.

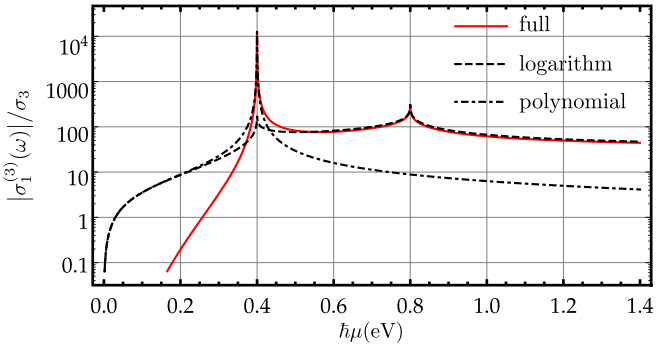

FIG. 6. Optical Kerr conductivity: The role of logarithmic divergences and polynomial resonances. We set $\hbar\omega = 800$ meV in graphene ($\Delta \to 0$) as a function of doping. The solid red curve represents the complete solution of Eq. (C2) and black curves represent the contributions from logarithmic divergences (dashed) and polynomial resonances (dotted-dashed).

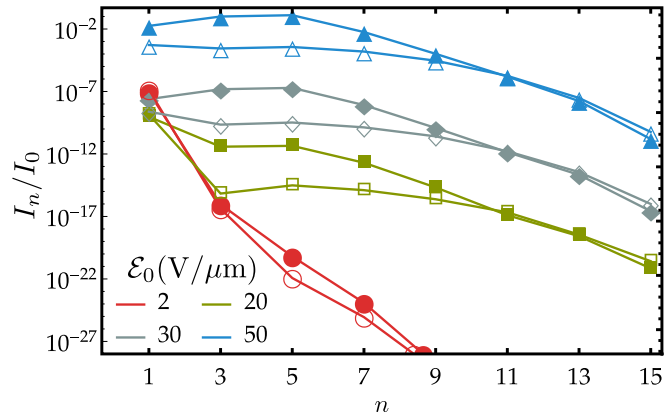

FIG. 7. The role of doping in the nonlinear response. Relative intensity of the nth Fourier components of the field radiated by the current response in doped graphene, $\hbar\mu = \{250, 312.5\}$ meV, solid and open symbols, respectively, considering an external monochromatic field with photon energy $\hbar\omega = 100$ meV and intensity in vacuum $I_0 = \varepsilon_0 c_0 \mathcal{E}_0^2/2$.

$j_n(\omega) = \sum_j \sigma_n^{(j)}(\omega)\mathcal{E}_0^j$ with respect to the incident intensity in vacuum $I_0 = \varepsilon_0 c_0 \mathcal{E}_0^2/2$ [44,45] considering all contributions up to $j = 15$. Note that the analytic expressions for the conductivities are limited to ninth order, hence all data plotted in Fig. 5 were integrated numerically using $\hbar\eta = 10$ meV. Results shown in Figs. 2–5 demonstrate that the approach presented in this paper can be used to readily characterize the harmonic response of graphene, including the effects from higher-order terms, at arbitrary doping level and photon frequency, without requiring the complex numerical calculations found in time-dependent techniques.

In summary, we introduce an iterative approach to the calculation of NLO response of systems described by the massive Dirac Hamiltonian. The iterative nature allows for an analytical evaluation of high-order response functions, and we derive all nonlinear conductivities of (gapped) graphene up to ninth order. Small band gaps play an important role in lightly doped graphene, amplifying considerably the NLO response at low photon energy. Moreover, results for higher-order processes, e.g., FHG, show that the nth-order response of graphene contains n logarithmic resonances. The interplay between doping, photon energy, and the optical intensity is illustrated by results for high-harmonic generation.

The authors acknowledge Alireza Taghizadeh for many helpful comments. This work was supported by the QUSCOPE center sponsored by the Villum Foundation, and TGP is supported by the CNG center under the Danish National Research Foundation, Project No. DNRF103.

APPENDIX A: INTERPLAY BETWEEN LOGARITHMIC AND POLYNOMIAL PARTS

The polynomial resonances found in higher-order contributions to a given Fourier component, i.e., $j > n$, play an important role in the overall response of the system, by enhancing significantly the $(j + n - 2)/2$ lowest resonances. To illustrate this, we plot in Fig. 6 the contributions that arise from the logarithmic divergences and from the polynomial resonances in the optical Kerr conductivity $\sigma_1^{(3)}(\omega)$. The effect is twofold: First and most striking is the dramatic increase in the amplitude of the lowest resonance by virtue of the polynomial resonance. Second is the destructive combination of both contributions for small doping $\mu < \omega/2$.

APPENDIX B: HIGHER-ORDER TERMS AND ROLE OF DOPING

Doping plays an important role in the optical response of graphene. At linear order its effect is well know, primarily blocking the real part of the response for $\omega < 2\mu$ and sets the amplitude of the Drude peak. Yet, as discussed above and in the main text (see Fig. 2), its role in the nonlinear response can be drastic. In Fig. 7, we plot the amplitude of the Fourier components of the radiated field at two different doping levels $\hbar\mu = \{250, 312.5\}$ meV. Despite the relatively small change in doping, the nonlinear response changes drastically, particularly the Fourier components $n = \{3, 5, 7\}$, stressing once more the importance of the interplay between doping level and photon energy.

TABLE II. Coefficients q_{nj} for nonlinear conductivities of graphene at the zero doping limit.

n	$j=1$	3	5	7	9
1	1	45/256	1629/16384	1708371/10485760	41182970949/134217728000
3		3/512	−351/32768	−30475581/838860800	−11749230389433/1342177280000
5			−45/65536	777122073/262144000	−1205821487213379/164416716800000
7				7371/104857600	−1251787974784857/460366807040000
9					−3971997/751619276800

APPENDIX C: CONDUCTIVITIES UP TO NINTH ORDER FOR GAPPED SYSTEMS

The general expressions for the nth-harmonic and higher-order corrections $j > n$ in gapped graphene can be expressed in the form

$$\sigma_n^{(n)}(\omega) = \frac{i\sigma_n}{\pi}\left(\frac{2v_F}{3a_0\omega}\right)^{2(n-1)} \sum_{m=1}^{n} \ln\frac{2\Omega - m\omega}{2\Omega + m\omega} \sum_{k=0}^{(n+1)/2} c_{km}^{(nn)}\left(\frac{\Delta}{\omega}\right)^{2k}, \tag{C1a}$$

$$\sigma_n^{(j)}(\omega) = \frac{i\sigma_j}{\pi}\left(\frac{2v_F}{3a_0\omega}\right)^{2(j-1)}\left[\sum_{m=1}^{(n+j)/2} \ln\frac{2\Omega - m\omega}{2\Omega + m\omega} \sum_{k=0}^{(j+1)/2} c_{km}^{(nj)}\left(\frac{\Delta}{\omega}\right)^{2k} + \frac{P_{nj}}{Q_{nj}}\right] \quad (j > n), \tag{C1b}$$

where $c_{km}^{(nj)}$ are constant coefficients, P_{nj} and Q_{nj} are polynomial functions in ω, and recall the systematic definition of the nonlinear conductivity scales introduced in the main text, $\sigma_{j>1} \equiv 2[3ea_0/(4\hbar v_F)]^{j-1}\sigma_1$. As shown in Eq. (11) in the main text, all nonlinear conductivities are regular at vanishing doping. The complete list of nonzero coefficients q_{nj}, up to ninth order, can be found in Table II.

We provide the full expressions for the optical Kerr effect, fifth-, seventh-, and ninth-harmonic conductivities, namely, Eqs. (C2)–(C5). For $j > n$, we provide the coefficients $c_{km}^{(nj)}$ in Table III and the respective polynomial functions P_{nj} and Q_{nj}, found in Eqs. (C6) and (C7). Results for gapless graphene can be expressed directly from those of gapped graphene, by taking the limit $\Delta \to 0$ and replacing Ω by μ.

The optical Kerr conductivity in gapped graphene reads

$$\begin{aligned}\sigma_1^{(3)}(\omega) = \frac{9i\sigma_3}{256\pi}\left(\frac{2v_F}{3a_0\omega}\right)^4\Bigg[&\frac{4[3\Omega^2\omega^4 + 8\Delta^2\Omega^2\omega^2 + 48\Delta^4(9\Omega^2 - 2\omega^2)]}{\omega^3\mu(4\mu^2 - \omega^2)} \\ &+\left(16 + \frac{32\Delta^2}{\omega^2} - \frac{48\Delta^4}{\omega^4}\right)\ln\frac{2\omega - 2\Omega}{2\omega + 2\Omega} - \left(11 + \frac{56\Delta^2}{\omega^2} - \frac{5283\Delta^4}{\omega^4}\right)\ln\frac{\omega - 2\Omega}{\omega + 2\Omega}\Bigg].\end{aligned} \tag{C2}$$

The fifth-, seventh-, and ninth-harmonic conductivities read

$$\begin{aligned}\sigma_5^{(5)}(\omega) = \frac{9i\sigma_5}{655360\pi}\left(\frac{2v_F}{3a_0\omega}\right)^8\Bigg[&\left(4925 + \frac{3788\Delta^2}{\omega^2} - \frac{2640\Delta^4}{\omega^4} + \frac{320\Delta^6}{\omega^6}\right)\ln\frac{2\Omega - 5\omega}{2\Omega + 5\omega} \\ &-\left(16384 + \frac{16384\Delta^2}{\omega^2} - \frac{15360\Delta^4}{\omega^4} + \frac{2560\Delta^6}{\omega^6}\right)\ln\frac{2\Omega - 4\omega}{2\Omega + 4\omega} \\ &+\left(19359 + \frac{27396\Delta^2}{\omega^2} - \frac{36720\Delta^4}{\omega^4} + \frac{8640\Delta^6}{\omega^6}\right)\ln\frac{2\Omega - 3\omega}{2\Omega + 3\omega} \\ &-\left(9216 + \frac{21504\Delta^2}{\omega^2} - \frac{46080\Delta^4}{\omega^4} + \frac{15360\Delta^6}{\omega^6}\right)\ln\frac{2\Omega - 2\omega}{2\Omega + 2\omega} \\ &+\left(1266 + \frac{7416\Delta^2}{\omega^2} - \frac{30240\Delta^4}{\omega^4} + \frac{13440\Delta^6}{\omega^6}\right)\ln\frac{2\Omega - \omega}{2\Omega + \omega}\Bigg],\end{aligned} \tag{C3}$$

$$\begin{aligned}\sigma_7^{(7)}(\omega) = \frac{i\sigma_7}{2936012800\pi}\left(\frac{2v_F}{3a_0\omega}\right)^{12}\Bigg[&-\left(5126429 + \frac{2911408\Delta^2}{\omega^2} - \frac{1680672\Delta^4}{\omega^4} + \frac{224000\Delta^6}{\omega^6} - \frac{8960\Delta^8}{\omega^8}\right)\ln\frac{2\Omega - 7\omega}{2\Omega + 7\omega} \\ &+\left(27122688 + \frac{18468864\Delta^2}{\omega^2} - \frac{13031424\Delta^4}{\omega^4} + \frac{2150400\Delta^6}{\omega^6} - \frac{107520\Delta^8}{\omega^8}\right)\ln\frac{2\Omega - 6\omega}{2\Omega + 6\omega} \\ &-\left(58448125 + \frac{49425200\Delta^2}{\omega^2} - \frac{43925280\Delta^4}{\omega^4} + \frac{9184000\Delta^6}{\omega^6} - \frac{582400\Delta^8}{\omega^8}\right)\ln\frac{2\Omega - 5\omega}{2\Omega + 5\omega} \\ &+\left(65011712 + \frac{71827456\Delta^2}{\omega^2} - \frac{83951616\Delta^4}{\omega^4} + \frac{22937600\Delta^6}{\omega^6} - \frac{1863680\Delta^8}{\omega^8}\right)\ln\frac{2\Omega - 4\omega}{2\Omega + 4\omega} \\ &-\left(38624121 + \frac{60454512\Delta^2}{\omega^2} - \frac{99273888\Delta^4}{\omega^4} + \frac{36960000\Delta^6}{\omega^6} - \frac{3843840\Delta^8}{\omega^8}\right)\ln\frac{2\Omega - 3\omega}{2\Omega + 3\omega} \\ &+\left(11127808 + \frac{28676096\Delta^2}{\omega^2} - \frac{74102784\Delta^4}{\omega^4} + \frac{39424000\Delta^6}{\omega^6} - \frac{5125120\Delta^8}{\omega^8}\right)\ln\frac{2\Omega - 2\omega}{2\Omega + 2\omega} \\ &-\left(1040601 + \frac{6605808\Delta^2}{\omega^2} - \frac{32987808\Delta^4}{\omega^4} + \frac{25132800\Delta^6}{\omega^6} - \frac{3843840\Delta^8}{\omega^8}\right)\ln\frac{2\Omega - \omega}{2\Omega + \omega}\Bigg],\end{aligned} \tag{C4}$$

TABLE III. Coefficients $c_{km}^{(nj)}$ for nonlinear response functions.

(n, j, m)	$k=0$	1	2	3	4	5
(1,5,1)	10701/32768	34947/8192	−483381/2048	969525/512		
(1,5,2)	−45/32	−153/32	1161/32	−1395/32		
(1,5,3)	38637/32768	14499/8192	−5589/2048	405/512		
(1,7,1)	3600747/20971520	−6782823/1310720	169399269/131072	−651055779/16384	3945678975/16384	
(1,7,2)	136161/20480	73161/5120	−323757/2048	905553/1024	−4359915/4096	
(1,7,3)	−167924421/20971520	−15788439/1310720	3105621/131072	−243027/16384	59535/16384	
(1,7,4)	27/20	261/160	−567/256	189/256	−315/4096	
(1,9,1)	−536495434947/33554432000	−88185569733/1048576000	−4189625617617/1048576000	2120218804413/5242880	−192284854599159/26214400	55631582404839/1638400
(1,9,2)	−3050307/81920	190719/40960	−36570717/204800	−17693703/5120	1775845197/81920	−5334749343/204800
(1,9,3)	642944283021/10737418240	249472395639/2684354560	−219108549339/1677721600	−986683977/83886080	1749025089/41943040	−395538633/52428800
(1,9,4)	−58293/8000	−67689/8000	1595349/128000	−14769/2560	268947/204800	−101493/819200
(1,9,5)	2015654625/2147483648	507577995/536870912	−377403543/335544320	6149115/16777216	−415611/8388608	5103/2097152
(3,5,1)	9645/65536	14811/16384	−76581/4096	49965/1024		
(3,5,2)	−135/128	−243/128	1107/128	−1305/128		
(3,5,3)	83349/65536	25299/16384	−9549/4096	885/1024		
(3,5,4)	−3/8	−3/8	45/128	−15/256		
(3,7,1)	−53626869/209715200	−87837/51200	823121811/6553600	−32860899/16384	831053307/163840	
(3,7,2)	603219/102400	234537/25600	−1875591/51200	165441/1024	−4318377/20480	
(3,7,3)	−12590778429/1677721600	−994320873/104857600	599493141/52428800	−582069/262144	611247/1310720	
(3,7,4)	57/25	3609/1600	−34947/12800	483/512	−4767/40960	
(3,7,5)	−29980125/67108864	−1603665/4194304	3655449/10485760	−19845/262144	1323/262144	
(3,9,1)	−986591420139/335544320000	−437837072259/41943040000	−4257643835421/10485760000	877567678881/32768000	−76700693056071/262144000	108776910373047/163840000
(3,9,2)	−636647541/16384000	−801618267/16384000	284929479/8192000	−161264883/327680	11771307723/3276800	−628424811/131072
(3,9,3)	165604667600259/3758096384000	57586714680177/939524096000	−1054096281783/16777216000	−10238869521/167772160	32777476869/419430400	−82088937/4194304
(3,9,4)	−3703851/896000	−1131831/358400	6934797/2560000	−3313287/4096000	9481401/32768000	−4836321/81920000
(3,9,5)	8794901025/4294967296	1856912067/1073741824	−6048576099/3355443200	470971179/838860800	−6728967/83886080	2366091/524288000
(3,9,6)	−24938361/81920000	−18784143/81920000	8067843/40960000	−371763/8192000	70119/16384000	−11907/81920000
(5,7,1)	−42084549/1048576000	−18675387/65536000	244263681/32768000	−4560003/163840	10682847/819200	
(5,7,2)	55539/81920	24921/20480	−46251/8192	37125/4096	−53865/16384	
(5,7,3)	−31324401/20971520	−152361/81920	421767/131072	−15525/8192	6615/16384	
(5,7,4)	5463/4000	10593/8000	−49437/32000	2637/5120	−12789/204800	
(5,7,5)	−5255505/8388608	−1311021/2621440	14508693/32768000	−16353/163840	6111/819200	
(5,7,6)	238383/2048000	40581/512000	−57267/1024000	189/20480	−189/409600	
(5,9,1)	577353118113/4110417920000	2638802199357/4110417920000	−48508858079019/1284505600000	14516873633097/18350080000	−235727258373/81920000	15796816546743/11468800000
(5,9,2)	−3998224989/802816000	−6288282153/802816000	6780010203/401408000	−935238663/11468800	109778031/655360	−7597555947/114688000
(5,9,3)	1729523840823/268435456000	3980375587593/469762048000	−462887122311/58720256000	−2456297433/419430400	1020541167/209715200	−178915797/262144000
(5,9,4)	−9642843/3200000	−108121941/44800000	192500793/89600000	−10960173/20480000	20177523/163840000	−10064979/409600000
(5,9,5)	1039550600547/526133493760	5087867850423/3288334336000	−15344124829389/10276044800000	32162212953/73400320000	−329176917/5242880000	180046557/45875200000
(5,9,6)	−13064400981/20070400000	−9073263033/20070400000	3707954739/10035200000	−4888539/57344000	700947/81920000	−187839/573440000
(5,9,7)	6079966893/67108864000	936300519/16777216000	−563601753/14680064000	732699/104857600	−27027/52428800	891/65536000
(7,9,1)	6230389014279/920733614080000	12156373280043/230183403520000	−43104455194473/28772925440000	1361662428573/205520896000	−15649268877/2936012800	108596636577/128450560000
(7,9,2)	−1230921/6553600	−15871743/45875200	35218017/22937600	−1843497/655360	2153151/1310720	−1517373/6553600
(7,9,3)	219591204687/375809638400	14174937711/18790481920	−16040957553/11744051200	77976621/83886080	−12826863/41943040	1740609/52428800
(7,9,4)	−991017/1120000	−1978677/2240000	20060973/17920000	−934083/2048000	18459/204800	−1123551/163840000
(7,9,5)	1746312975/2147483648	2487748509/3758096384	−7662410271/11744051200	79887807/419430400	−1070433/41943040	353403/262144000
(7,9,6)	−25577684523/56197120000	−17569607859/56197120000	7051200741/28098560000	−45480069/802816000	255609/45875200	−1688121/8028160000
(7,9,7)	3075199281/21474836480	15978363687/187904819200	−65786982381/1150917017600	85423473/8220835840	−462501/587202560	113157/5138022400
(7,9,8)	−2673/137200	−5589/548800	41067/7024640	−7047/8028160	243/4587520	−729/642252800

$$\sigma_9^{(9)}(\omega) = \frac{27i\sigma_9}{10522669875200\pi}\left(\frac{2v_F}{3a_0\omega}\right)^{16}\Bigg[\Bigg(811948293 + \frac{369488004\Delta^2}{\omega^2} - \frac{182320480\Delta^4}{\omega^4} + \frac{23327360\Delta^6}{\omega^6} - \frac{1191680\Delta^8}{\omega^8} + \frac{21504\Delta^{10}}{\omega^{10}}\Bigg)\ln\frac{2\Omega-9\omega}{2\Omega+9\omega} - \Bigg(5905580032 + \frac{3087007744\Delta^2}{\omega^2} - \frac{1772093440\Delta^4}{\omega^4} + \frac{266076160\Delta^6}{\omega^6} - \frac{16056320\Delta^8}{\omega^8} + \frac{344064\Delta^{10}}{\omega^{10}}\Bigg)\ln\frac{2\Omega-8\omega}{2\Omega+8\omega} + \Bigg(18559737203 + \frac{11360173916\Delta^2}{\omega^2} - \frac{7720364960\Delta^4}{\omega^4} + \frac{1381063040\Delta^6}{\omega^6} - \frac{99662080\Delta^8}{\omega^8} + \frac{2558976\Delta^{10}}{\omega^{10}}\Bigg)\ln\frac{2\Omega-7\omega}{2\Omega+7\omega} - \Bigg(32794509312 + \frac{24102076416\Delta^2}{\omega^2} - \frac{19837419520\Delta^4}{\omega^4} + \frac{4309975040\Delta^6}{\omega^6} - \frac{377323520\Delta^8}{\omega^8} + \frac{11698176\Delta^{10}}{\omega^{10}}\Bigg)\ln\frac{2\Omega-6\omega}{2\Omega+6\omega} + \Bigg(35426172500 + \frac{32354387600\Delta^2}{\omega^2} - \frac{33255536000\Delta^4}{\omega^4} + \frac{8998976000\Delta^6}{\omega^6} - \frac{972160000\Delta^8}{\omega^8} + \frac{36556800\Delta^{10}}{\omega^{10}}\Bigg)\ln\frac{2\Omega-5\omega}{2\Omega+5\omega} - \Bigg(23722983424 + \frac{28303163392\Delta^2}{\omega^2} - \frac{37947965440\Delta^4}{\omega^4} + \frac{13230407680\Delta^6}{\omega^6} - \frac{1798307840\Delta^8}{\omega^8} + \frac{81887232\Delta^{10}}{\omega^{10}}\Bigg)\ln\frac{2\Omega-4\omega}{2\Omega+4\omega} + \Bigg(9439968636 + \frac{15933700272\Delta^2}{\omega^2} - \frac{29786529920\Delta^4}{\omega^4} + \frac{14022561280\Delta^6}{\omega^6} - \frac{2442818560\Delta^8}{\omega^8} + \frac{133066752\Delta^{10}}{\omega^{10}}\Bigg)\ln\frac{2\Omega-3\omega}{2\Omega+3\omega} - \Bigg(1956020224 + \frac{5417893888\Delta^2}{\omega^2} - \frac{15830548480\Delta^4}{\omega^4} + \frac{10704977920\Delta^6}{\omega^6} - \frac{2400419840\Delta^8}{\omega^8} + \frac{152076288\Delta^{10}}{\omega^{10}}\Bigg)\ln\frac{2\Omega-2\omega}{2\Omega+2\omega} + \Bigg(139206806 + \frac{937313528\Delta^2}{\omega^2} - \frac{5333514560\Delta^4}{\omega^4} + \frac{5380094720\Delta^6}{\omega^6} - \frac{1488847360\Delta^8}{\omega^8} + \frac{104552448\Delta^{10}}{\omega^{10}}\Bigg)\ln\frac{2\Omega-\omega}{2\Omega+\omega}\Bigg]. \tag{C5}$$

The polynomial functions of the family P_{nj} read

$$P_{15} = -27[-320\Delta^6(6860\mu^8 - 9795\mu^6\omega^2 + 3149\mu^4\omega^4 - 216\mu^2\omega^6 - 16\omega^8) + 48\Delta^4(4340\mu^8\omega^2 - 6469\mu^6\omega^4 + 2297\mu^4\omega^6 - 240\mu^2\omega^8) - 4\Delta^2(4\mu^8\omega^4 + 343\mu^6\omega^6 - 59\mu^4\omega^8) - 1276\mu^8\omega^6 + 119\mu^6\omega^8 + 5\mu^4\omega^{10}], \tag{C6a}$$

$$P_{17} = 81[896\Delta^8(220725120\mu^{16} - 1085717600\mu^{14}\omega^2 + 1871794584\mu^{12}\omega^4 - 1439294370\mu^{10}\omega^6 + 506082893\mu^8\omega^8 - 77041635\mu^6\omega^{10} + 3399312\mu^4\omega^{12} + 20160\mu^2\omega^{14} + 20736\omega^{16}) - 1280\Delta^6\mu^2\omega^2(24602816\mu^{14} - 121233232\mu^{12}\omega^2 + 209561348\mu^{10}\omega^4 - 161682431\mu^8\omega^6 + 57044056\mu^6\omega^8 - 8625293\mu^4\omega^{10} + 300768\mu^2\omega^{12} + 27648\omega^{14}) + 96\Delta^4\mu^4\omega^4(8962240\mu^{12} - 44433104\mu^{10}\omega^2 + 77619556\mu^8\omega^4 - 60976999\mu^6\omega^6 + 22423706\mu^4\omega^8 - 3822343\mu^2\omega^{10} + 244224\omega^{12}) - 16\Delta^2\mu^6\omega^6(321472\mu^{10} - 1125392\mu^8\omega^2 + 964020\mu^6\omega^4 - 259267\mu^4\omega^6 + 27338\mu^2\omega^8 + 2709\omega^{10}) + \mu^6\omega^8(-4269376\mu^{10} + 16069552\mu^8\omega^2 - 16274748\mu^6\omega^4 + 7469521\mu^4\omega^6 - 1748206\mu^2\omega^8 + 135657\omega^{10})], \tag{C6b}$$

$$
\begin{aligned}
P_{19} = 27[&46080\Delta^{10}(187256945075200\mu^{26} - 2325179092531456\mu^{24}\omega^2 + 11687240067038592\mu^{22}\omega^4 \\
&- 31227635973633056\mu^{20}\omega^6 + 48860300608451540\mu^{18}\omega^8 - 46478022674034021\mu^{16}\omega^{10} \\
&+ 26989978924387315\mu^{14}\omega^{12} - 9364370227141651\mu^{12}\omega^{14} + 1846375279461405\mu^{10}\omega^{16} - 181530914846796\mu^8\omega^{18} \\
&+ 5430654668160\mu^6\omega^{20} + 169113692160\mu^4\omega^{22} - 15282266112\mu^2\omega^{24} + 3224862720\omega^{26}) \\
&- 8960\Delta^8\mu^2\omega^2(207124212399104\mu^{24} - 2572102733782784\mu^{22}\omega^2 + 12929922371094144\mu^{20}\omega^4 \\
&- 34553358155256544\mu^{18}\omega^6 + 54074328703809484\mu^{16}\omega^8 - 51449663244720339\mu^{14}\omega^{10} \\
&+ 29884780216342349\mu^{12}\omega^{12} - 10371651232074029\mu^{10}\omega^{14} + 2046000204112899\mu^8\omega^{16} - 202081754607804\mu^6\omega^{18} \\
&+ 6770075385600\mu^4\omega^{20} - 102269952000\mu^2\omega^{22} + 35473489920\omega^{24}) + 3200\Delta^6\mu^4\omega^4(31610284073984\mu^{22} \\
&- 392635665455360\mu^{20}\omega^2 + 1974400862745984\mu^{18}\omega^4 - 5278454843537440\mu^{16}\omega^6 + 8264714267791444\mu^{14}\omega^8 \\
&- 7868286992375685\mu^{12}\omega^{10} + 4573179204764219\mu^{10}\omega^{12} - 1587286528597115\mu^8\omega^{14} + 311808898399989\mu^6\omega^{16} \\
&- 29677946203620\mu^4\omega^{18} + 559840481280\mu^2\omega^{20} + 67124920320\omega^{22}) - 96\Delta^4\mu^6\omega^6(12461343792128\mu^{20} \\
&- 153934549591808\mu^{18}\omega^2 + 768680423211648\mu^{16}\omega^4 \\
&- 2037737318722528\mu^{14}\omega^6 + 3159909982948588\mu^{12}\omega^8 - 2978876192190843\mu^{10}\omega^{10} + 1718919063655493\mu^8\omega^{12} \\
&- 598137631786373\mu^6\omega^{14} + 121291455245643\mu^4\omega^{16} - 13131969585948\mu^2\omega^{18} + 585252864000\omega^{20}) \\
&+ 4\Delta^2\mu^8\omega^8(11128861893632\mu^{18} - 128298690021632\mu^{16}\omega^2 + 584308470525312\mu^{14}\omega^4 - 1375544099233312\mu^{12}\omega^6 \\
&+ 1838156397364372\mu^{10}\omega^8 - 1446756964610997\mu^8\omega^{10} + 672490048294667\mu^6\omega^{12} - 180284596846667\mu^4\omega^{14} \\
&+ 25742523524517\mu^2\omega^{16} - 1539147689892\omega^{18}) + \mu^8\omega^{10}(16473311681536\mu^{18} - 185685695854336\mu^{16}\omega^2 \\
&+ 820185567144576\mu^{14}\omega^4 - 1854452838481376\mu^{12}\omega^6 + 2358902774973356\mu^{10}\omega^8 - 1755059863889931\mu^8\omega^{10} \\
&+ 760761649666741\mu^6\omega^{12} - 187368464362741\mu^4\omega^{14} + 24210354003291\mu^2\omega^{16} - 1311096961116\omega^{18})], \qquad \text{(C6c)}
\end{aligned}
$$

$$
\begin{aligned}
P_{35} = 9[&1600\Delta^6(140\mu^6 - 495\mu^4\omega^2 + 439\mu^2\omega^4 - 72\omega^6) + 48\Delta^4\omega^2(-1060\mu^6 + 3837\mu^4\omega^2 - 3593\mu^2\omega^4 + 576\omega^6) \\
&+4\Delta^2(436\mu^6\omega^4 - 1009\mu^4\omega^6 - 387\mu^2\omega^8) + \mu^2\omega^6(2572\mu^4 - 7231\mu^2\omega^2 + 819\omega^4)], \qquad \text{(C6d)}
\end{aligned}
$$

$$
\begin{aligned}
P_{37} = 9[&8960\Delta^8(154842688\mu^{16} - 1693862192\mu^{14}\omega^2 + 7076655628\mu^{12}\omega^4 - 14432352001\mu^{10}\omega^6 + 15117336290\mu^8\omega^8 \\
&- 7801203157\mu^6\omega^{10} + 1676409144\mu^4\omega^{12} - 92253600\mu^2\omega^{14} - 6220800\omega^{16}) + 6400\Delta^6\omega^2(-78564416\mu^{16} \\
&+ 861403824\mu^{14}\omega^2 - 3610618540\mu^{12}\omega^4 + 7397960105\mu^{10}\omega^6 - 7800557442\mu^8\omega^8 + 4065811129\mu^6\omega^{10} \\
&- 894421668\mu^4\omega^{12} + 57514752\mu^2\omega^{14} + 1990656\omega^{16}) + 96\Delta^4\mu^2\omega^4(240655296\mu^{14} - 2644591184\mu^{12}\omega^2 \\
&+ 11132594516\mu^{10}\omega^4 - 22987069287\mu^8\omega^6 + 24527909390\mu^6\omega^8 - 13001424359\mu^4\omega^{10} + 2981172348\mu^2\omega^{12} \\
&- 238878720\omega^{14}) - 16\Delta^2\mu^4\omega^6(88161088\mu^{12} - 833246704\mu^{10}\omega^2 + 2795912700\mu^8\omega^4 - 4054626277\mu^6\omega^6 \\
&+ 2413067146\mu^4\omega^8 - 488748069\mu^2\omega^{10} + 38008116\omega^{12}) + \mu^4\omega^8(-1223424832\mu^{12} + 11825233648\mu^{10}\omega^2 \\
&- 41147030652\mu^8\omega^4 + 62929802869\mu^6\omega^6 - 41214902890\mu^4\omega^8 + 10669588533\mu^2\omega^{10} - 1009826676\omega^{12})], \qquad \text{(C6e)}
\end{aligned}
$$

$$
\begin{aligned}
P_{39} = 9[&64512\Delta^{10}(309753515495424\mu^{28} - 7641740299675648\mu^{26}\omega^2 + 80412581120246528\mu^{24}\omega^4 \\
&- 475750643401113088\mu^{22}\omega^6 + 1754584695596524208\mu^{20}\omega^8 - 4223937570253353928\mu^{18}\omega^{10} \\
&+ 6751925001676414493\mu^{16}\omega^{12} - 7145124722011657483\mu^{14}\omega^{14} + 4898503653386626283\mu^{12}\omega^{16} \\
&- 2080663453422856033\mu^{10}\omega^{18} + 505895262262389564\mu^8\omega^{20} - 60849869183824320\mu^6\omega^{22} \\
&+ 2320230220416000\mu^4\omega^{24} + 4237671168000\mu^2\omega^{26} + 12093235200000\omega^{28}) - 8960\Delta^8\omega^2(972060393148416\mu^{28} \\
&- 23984147489032192\mu^{26}\omega^2 + 252421208707688192\mu^{24}\omega^4 - 1493720153089864192\mu^{22}\omega^6 \\
&+ 5510291747508277232\mu^{20}\omega^8 - 13269530175856290472\mu^{18}\omega^{10} + 21219569657598491417\mu^{16}\omega^{12} \\
&- 22466131756544682187\mu^{14}\omega^{14} + 15411021721264809947\mu^{12}\omega^{16} - 6549877232232901057\mu^{10}\omega^{18} \\
&+ 1592687514214980096\mu^8\omega^{20} - 190486298653441200\mu^6\omega^{22} + 6526133560627200\mu^4\omega^{24} + 218411889868800\mu^2\omega^{26} \\
&+ 19349176320000\omega^{28}) + 640\Delta^6\mu^2\omega^4(1222308154912768\mu^{26} - 30167798532724736\mu^{24}\omega^2 \\
&+ 317620928184714496\mu^{22}\omega^4 - 1880414993390921216\mu^{20}\omega^6 + 6940699972336059856\mu^{18}\omega^8 \\
&- 16725442627223072696\mu^{16}\omega^{10} + 26767586681448735451\mu^{14}\omega^{12} - 28367813457999362681\mu^{12}\omega^{14} \\
&+ 19484307833540761081\mu^{10}\omega^{16} - 8298098342699425131\mu^8\omega^{18}
\end{aligned}
$$

$$+ 2026708139492503848\mu^6\omega^{20} - 24508963157458104\mu^4\omega^{22} + 8437345689600000\mu^2\omega^{24} + 451480780800000\omega^{26})$$
$$-480\Delta^4\mu^4\omega^6(33211897040896\mu^{24} - 812271998609408\mu^{22}\omega^2 + 8458992945701632\mu^{20}\omega^4$$
$$- 49438723339383296\mu^{18}\omega^6 + 179773666199270320\mu^{16}\omega^8 - 425870027861226824\mu^{14}\omega^{10}$$
$$+ 668539751184633373\mu^{12}\omega^{12} - 693525260286524207\mu^{10}\omega^{14} + 465737013219803311\mu^8\omega^{16}$$
$$- 194382587913945165\mu^6\omega^{18} + 47152930812034968\mu^4\omega^{20} - 5973952612395600\mu^2\omega^{22}$$
$$+ 300987187200000\omega^{24}) + 4\Delta^2\mu^6\omega^8(536217522040832\mu^{22} - 12496633825982464\mu^{20}\omega^2$$
$$+ 122387461446996224\mu^{18}\omega^4 - 661840153597033984\mu^{16}\omega^6 + 2181946355016020624\mu^{14}\omega^8$$
$$- 4567485492086789464\mu^{12}\omega^{10} + 6132062217877668239\mu^{10}\omega^{12} - 5217351621756729589\mu^8\omega^{14}$$
$$+ 2723231065199668469\mu^6\omega^{16} - 822367121180168799\mu^4\omega^{18} + 130218923351183112\mu^2\omega^{20}$$
$$- 8214161326873200\omega^{22}) + \mu^6\omega^{10}(1326111826087936\mu^{22} - 30780984984061952\mu^{20}\omega^2$$
$$+ 299899605136498432\mu^{18}\omega^4 - 1611098752492186112\mu^{16}\omega^6 + 5266492798707198832\mu^{14}\omega^8$$
$$- 10904888055843848552\mu^{12}\omega^{10} + 14444414998165145377\mu^{10}\omega^{12} - 12103980506737587227\mu^8\omega^{14}$$
$$+ 6224529344696909467\mu^6\omega^{16} - 1854359645704647057\mu^4\omega^{18} + 290123422224942456\mu^2\omega^{20}$$
$$- 18166817810451600\omega^{22})], \tag{C6f}$$

$$P_{57} = -81[-62720\Delta^8(1232\mu^{10} - 17016\mu^8\omega^2 + 79737\mu^6\omega^4 - 150974\mu^4\omega^6 + 105921\mu^2\omega^8 - 16200\omega^{10})$$
$$+ 44800\Delta^6\omega^2(3184\mu^{10} - 44088\mu^8\omega^2 + 207555\mu^6\omega^4 - 396607\mu^4\omega^6 + 283956\mu^2\omega^8 - 43200\omega^{10})$$
$$+ 96\Delta^4\omega^4(-163408\mu^{10} + 2304744\mu^8\omega^2 - 11210793\mu^6\omega^4 + 22779541\mu^4\omega^6 - 18591684\mu^2\omega^8$$
$$+ 2764800\omega^{10}) + 16\Delta^2\mu^2\omega^6(103184\mu^8 - 1342344\mu^6\omega^2 + 5578101\mu^4\omega^4 - 7907441\mu^2\omega^6 - 60300\omega^8)$$
$$+ \mu^2\omega^8(1411888\mu^8 - 18802008\mu^6\omega^2 + 82255407\mu^4\omega^4 - 139348387\mu^2\omega^6 + 21260700\omega^8)], \tag{C6g}$$

$$P_{59} = 81[193536\Delta^{10}(95335871488\mu^{24} - 3474467149056\mu^{22}\omega^2 + 53617091508608\mu^{20}\omega^4 - 459325309409696\mu^{18}\omega^6$$
$$+ 2406126551013348\mu^{16}\omega^8 - 8003718707211601\mu^{14}\omega^{10} + 17005840241750653\mu^{12}\omega^{12} - 22640508616620861\mu^{10}\omega^{14}$$
$$+ 18005536929127403\mu^8\omega^{16} - 7798933351991286\mu^6\omega^{18} + 1518142836231000\mu^4\omega^{20} - 78654784320000\mu^2\omega^{22}$$
$$- 5143824000000\omega^{24}) + 62720\Delta^8\omega^2(-598343263232\mu^{24} + 21811826077952\mu^{22}\omega^2 - 336705405969792\mu^{20}\omega^4$$
$$+ 2885724235393312\mu^{18}\omega^6 - 15125197416086932\mu^{16}\omega^8 + 50350676794142877\mu^{14}\omega^{10}$$
$$- 107091761127166907\mu^{12}\omega^{12} + 142772361431828627\mu^{10}\omega^{14} - 113757742393642437\mu^8\omega^{16}$$
$$+ 49407479442609732\mu^6\omega^{18} - 9674380682323200\mu^4\omega^{20} + 522367574400000\mu^2\omega^{22} + 29393280000000\omega^{24})$$
$$- 4480\Delta^6\omega^4(-2021660253184\mu^{24} + 73794708322048\mu^{22}\omega^2 - 1141127989167744\mu^{20}\omega^4$$
$$+ 9802241047129568\mu^{18}\omega^6 - 51531857164633964\mu^{16}\omega^8 + 172232438007379083\mu^{14}\omega^{10}$$
$$- 368281343263186729\mu^{12}\omega^{12} + 494471670546894313\mu^{10}\omega^{14} - 397667689343865879\mu^8\omega^{16}$$
$$+ 174906664504972488\mu^6\omega^{18} - 35123521332150000\mu^4\omega^{20} + 2226207836160000\mu^2\omega^{22} + 53747712000000\omega^{24})$$
$$- 96\Delta^4\mu^2\omega^6(3797717957632\mu^{22} - 137353886787328\mu^{20}\omega^2 + 2100673426799232\mu^{18}\omega^4$$
$$- 17812683917478368\mu^{16}\omega^6 + 92275903921064012\mu^{14}\omega^8 - 303537823856362203\mu^{12}\omega^{10}$$
$$+ 638808180919849177\mu^{10}\omega^{12} - 845617510364262553\mu^8\omega^{14} + 672165401963704647\mu^6\omega^{16}$$
$$- 292283205453447048\mu^4\omega^{18} + 58403636668162800\mu^2\omega^{20} - 4138573824000000\omega^{22})$$
$$+ 4\Delta^2\mu^4\omega^8(22851662222336\mu^{20} - 794742870529280\mu^{18}\omega^2 + 11536344229520256\mu^{16}\omega^4$$
$$- 91165811890041760\mu^{14}\omega^6 + 428772403776990916\mu^{12}\omega^8 - 1232248577574701265\mu^{10}\omega^{10}$$
$$+ 2137943903760337931\mu^8\omega^{12} - 2133108076863341195\mu^6\omega^{14} + 1110660721547411061\mu^4\omega^{16}$$
$$- 256938447392559000\mu^2\omega^{18} + 21939596325090000\omega^{20}) + \mu^4\omega^{10}(60324192345088\mu^{20} - 2104270345527040\mu^{18}\omega^2$$
$$+ 30665663343838848\mu^{16}\omega^4 - 243615590722170080\mu^{14}\omega^6 + 1154223486667714028\mu^{12}\omega^8$$
$$- 3351601703029398195\mu^{10}\omega^{10} - 5989529637878143585\mu^6\omega^{14} + 5896994399270064673\mu^8\omega^{12}$$
$$+ 3195062570596924863\mu^4\omega^{16} - 775441141395078600\mu^2\omega^{18} + 69308496112230000\omega^{20})], \tag{C6h}$$

$$
\begin{aligned}
P_{79} = 243[&9225216\Delta^{10}(8640\mu^{14} - 303056\mu^{12}\omega^2 + 4051828\mu^{10}\omega^4 - 26153487\mu^8\omega^6 + 85235078\mu^6\omega^8 - 133654567\mu^4\omega^{10} \\
&+ 85633164\mu^2\omega^{12} - 12700800\omega^{14}) + 3449600\Delta^8\omega^2(-135616\mu^{14} + 4759504\mu^{12}\omega^2 - 63690100\mu^{10}\omega^4 \\
&+ 411704335\mu^8\omega^6 - 1345235830\mu^6\omega^8 + 2119957831\mu^4\omega^{10} - 1372908924\mu^2\omega^{12} + 203212800\omega^{14}) \\
&+ 4480\Delta^6\omega^4(102146880\mu^{14} - 3592164848\mu^{12}\omega^2 + 48223006204\mu^{10}\omega^4 - 313372930341\mu^8\omega^6 \\
&+ 1033472807954\mu^6\omega^8 - 1657461145741\mu^4\omega^{10} + 1115180164692\mu^2\omega^{12} - 164195942400\omega^{14}) \\
&+ 96\Delta^4\omega^6(-283275456\mu^{14} + 10153353488\mu^{12}\omega^2 - 140346196932\mu^{10}\omega^4 + 955273089963\mu^8\omega^6 \\
&- 3398941352462\mu^6\omega^8 + 6190128382659\mu^4\omega^{10} - 5344783028460\mu^2\omega^{12} + 780337152000\omega^{14}) \\
&+ 4\Delta^2\mu^2\omega^8(1661793984\mu^{12} - 57125755280\mu^{10}\omega^2 + 739137628644\mu^8\omega^4 - 4506238654467\mu^6\omega^6 \\
&+ 13149352856702\mu^4\omega^8 - 16344830955483\mu^2\omega^{10} + 1129207092300\omega^{12}) + \mu^2\omega^{10}(4565365184\mu^{12} \\
&- 157885286352\mu^{10}\omega^2 + 2063250771828\mu^8\omega^4 - 12803179724687\mu^6\omega^6 + 38526000508278\mu^4\omega^8 \\
&- 57376387492551\mu^2\omega^{10} + 9431026271100\omega^{12})],
\end{aligned}
\tag{C6i}
$$

while the respective Q_{nj} polynomials read

$$Q_{15} = 512\omega^5\mu^3(4\mu^2 - 4\omega^2)(4\mu^2 - \omega^2)^2, \tag{C7a}$$

$$Q_{17} = 16384\omega^7\mu^5(4\mu^2 - 9\omega^2)(4\mu^2 - 4\omega^2)^2(4\mu^2 - \omega^2)^3, \tag{C7b}$$

$$Q_{19} = 6553600\omega^9\mu^7(4\mu^2 - 16\omega^2)(4\mu^2 - 9\omega^2)^2(4\mu^2 - 4\omega^2)^3(4\mu^2 - \omega^2)^4, \tag{C7c}$$

$$Q_{35} = 1024\omega^5\mu(4\mu^2 - 9\omega^2)(4\mu^2 - 4\omega^2)(4\mu^2 - \omega^2), \tag{C7d}$$

$$Q_{37} = 163840\omega^7\mu^3(4\mu^2 - 16\omega^2)(4\mu^2 - 9\omega^2)^2(4\mu^2 - 4\omega^2)^2(4\mu^2 - \omega^2)^2, \tag{C7e}$$

$$Q_{39} = 1048576000\omega^9\mu^5(4\mu^2 - 25\omega^2)(4\mu^2 - 16\omega^2)^2(4\mu^2 - 9\omega^2)^3(4\mu^2 - 4\omega^2)^3(4\mu^2 - \omega^2)^3, \tag{C7f}$$

$$Q_{57} = 819200\omega^7\mu(4\mu^2 - 25\omega^2)(4\mu^2 - 16\omega^2)(4\mu^2 - 9\omega^2)(4\mu^2 - 4\omega^2)(4\mu^2 - \omega^2), \tag{C7g}$$

$$Q_{59} = 18350080000\omega^9\mu^3(4\mu^2 - 36\omega^2)(4\mu^2 - 25\omega^2)^2(4\mu^2 - 16\omega^2)^2(4\mu^2 - 9\omega^2)^2(4\mu^2 - 4\omega^2)^2(4\mu^2 - \omega^2)^2, \tag{C7h}$$

$$Q_{79} = 10276044800\omega^9\mu(4\mu^2 - 49\omega^2)(4\mu^2 - 36\omega^2)(4\mu^2 - 25\omega^2)(4\mu^2 - 16\omega^2)(4\mu^2 - 9\omega^2)(4\mu^2 - 4\omega^2)(4\mu^2 - \omega^2). \tag{C7i}$$

[1] R. W. Boyd, *Nonlinear Optics*, 3rd ed. (Elsevier, Amsterdam, 2008).

[2] Y. R. Shen, *The Principles of Nonlinear Optics* (Wiley-Interscience, Hoboken, NJ, 2002).

[3] P. A. Franken and J. F. Ward, Rev. Mod. Phys. **35**, 23 (1963).

[4] N. Bloembergen, Rev. Mod. Phys. **54**, 685 (1982).

[5] V. M. Axt and S. Mukamel, Rev. Mod. Phys. **70**, 145 (1998).

[6] M. G. Kuzyk, K. D. Singer, and G. I. Stegeman, Adv. Opt. Photon. **5**, 4 (2013).

[7] A. Autere, H. Jussila, Y. Dai, Y. Wang, H. Lipsanen, and Z. Sun, Adv. Mater. **30**, 1705963 (2018).

[8] N. Yoshikawa, T. Tamaya, and K. Tanaka, Science **356**, 736 (2017).

[9] H. A. Hafez, S. Kovalev, J. C. Deinert, Z. Mics, B. Green, N. Awari, M. Chen, S. Germanskiy, U. Lehnert, J. Teichert, Z. Wang, K. J. Tielrooij, Z. Liu, Z. Chen, A. Narita, K. Müllen, M. Bonn, M. Gensch, and D. Turchinovich, Nature (London) **561**, 507 (2018).

[10] G.-K. Lim, Z.-L. Chen, J. Clark, R. G. S. Goh, W.-H. Ng, H.-W. Tan, R. H. Friend, P. K. H. Ho, and L.-L. Chua, Nat. Photon. **5**, 554 (2011).

[11] M. Mohsin, D. Neumaier, D. Schall, M. Otto, C. Matheisen, A. Lena Giesecke, A. A. Sagade, and H. Kurz, Sci. Rep. **5**, 10967 (2015).

[12] H. Liu, Y. Li, Y. S. You, S. Ghimire, T. F. Heinz, and D. A. Reis, Nat. Phys. **13**, 262 (2016).

[13] G. Soavi, G. Wang, H. Rostami, D. G. Purdie, D. De Fazio, T. Ma, B. Luo, J. Wang, A. K. Ott, D. Yoon, S. A. Bourelle, J. E. Muench, I. Goykhman, S. Dal Conte, M. Celebrano, A. Tomadin, M. Polini, G. Cerullo, and A. C. Ferrari, Nat. Nanotechnol. **13**, 583 (2018).

[14] T. Jiang, D. Huang, J. Cheng, X. Fan, Z. Zhang, Y. Shan, Y. Yi, Y. Dai, L. Shi, K. Liu, C. Zeng, J. Zi, J. E. Sipe, Y.-R. Shen, W.-T. Liu, and S. Wu, Nat. Photon. **12**, 430 (2018).

[15] Y. Zhang, D. Huang, Y. Shan, T. Jiang, Z. Zhang, K. Liu, L. Shi, J. Cheng, J. E. Sipe, W.-t. Liu, and S. Wu, Phys. Rev. Lett. **122**, 047401 (2019).

[16] G. Wang, X. Marie, I. Gerber, T. Amand, D. Lagarde, L. Bouet, M. Vidal, A. Balocchi, and B. Urbaszek, Phys. Rev. Lett. **114**, 097403 (2015).

[17] A. Säynätjoki, L. Karvonen, H. Rostami, A. Autere, S. Mehravar, A. Lombardo, R. A. Norwood, T. Hasan, N. Peyghambarian, H. Lipsanen, K. Kieu, A. C. Ferrari, M. Polini, and Z. Sun, Nat. Commun. **8**, 893 (2017).

[18] J. D. Cox, A. Marini, and F. J. G. de Abajo, Nat. Commun. **8**, 14380 (2017).

[19] D. Kundys, B. Van Duppen, O. P. Marshall, F. Rodriguez, I. Torre, A. Tomadin, M. Polini, and A. N. Grigorenko, Nano Lett. **18**, 282 (2018).

[20] Z. Wang, Z. Dong, H. Zhu, L. Jin, M.-H. Chiu, L.-J. Li, Q.-H. Xu, G. Eda, S. A. Maier, A. T. S. Wee, C.-W. Qiu, and J. K. W. Yang, ACS Nano **12**, 1859 (2018).
[21] D. S. Wild, E. Shahmoon, S. F. Yelin, and M. D. Lukin, Phys. Rev. Lett. **121**, 123606 (2018).
[22] G. Rosolen, L. J. Wong, N. Rivera, B. Maes, M. Soljačić, and I. Kaminer, Light: Sci. Appl. **7**, 64 (2018).
[23] C. Aversa and J. E. Sipe, Phys. Rev. B **52**, 14636 (1995).
[24] T. G. Pedersen, Phys. Rev. B **92**, 235432 (2015).
[25] A. Taghizadeh, F. Hipolito, and T. G. Pedersen, Phys. Rev. B **96**, 195413 (2017).
[26] F. Hipolito, A. Taghizadeh, and T. G. Pedersen, Phys. Rev. B **98**, 205420 (2018).
[27] J. L. Cheng, N. Vermeulen, and J. E. Sipe, New J. Phys. **16**, 053014 (2014).
[28] H. Rostami and M. Polini, Phys. Rev. B **93**, 161411(R) (2016).
[29] T. Tamaya, A. Ishikawa, T. Ogawa, and K. Tanaka, Phys. Rev. Lett. **116**, 016601 (2016).
[30] L. A. Chizhova, F. Libisch, and J. Burgdörfer, Phys. Rev. B **95**, 085436 (2017).
[31] D. Dimitrovski, T. G. Pedersen, and L. B. Madsen, Phys. Rev. A **95**, 063420 (2017).
[32] S. A. Mikhailov, Phys. Rev. B **95**, 085432 (2017).
[33] F. Catoire, H. Bachau, Z. Wang, C. Blaga, P. Agostini, and L. F. DiMauro, Phys. Rev. Lett. **121**, 143902 (2018).
[34] See Appendix C for the full expressions for gapped graphene and for additional information.
[35] G. W. Semenoff, Phys. Rev. Lett. **53**, 2449 (1984).
[36] N. M. R. Peres, Rev. Mod. Phys. **82**, 2673 (2010).
[37] A. H. Castro Neto, F. Guinea, N. M. R. Peres, K. S. Novoselov, and A. K. Geim, Rev. Mod. Phys. **81**, 109 (2009).
[38] D. Xiao, G.-B. Liu, W. Feng, X. Xu, and W. Yao, Phys. Rev. Lett. **108**, 196802 (2012).
[39] It is sufficient to consider $n \geqslant 0$, as the terms for $\mathcal{J}_{-n}^{(j)}$ can be immediately obtained from $\mathcal{J}_{n}^{(j)}$ by means of the replacement $\omega \to -\omega$.
[40] The discrete unit step function is defined as $\Theta_{i,j} = 1$ for $i \geqslant j$, $\Theta_{i,j} = 0$ for $i < j$.
[41] The integral over the wave vector has been replaced by an integration over energy.
[42] S. Y. Zhou, G.-H. Gweon, A. V. Fedorov, P. N. First, W. A. de Heer, D.-H. Lee, F. Guinea, A. H. Castro Neto, and A. Lanzara, Nat. Mater. **6**, 916 (2007).
[43] C. R. Woods, L. Britnell, A. Eckmann, R. S. Ma, J. C. Lu, H. M. Guo, X. Lin, G. L. Yu, Y. Cao, R. V. Gorbachev, A. V. Kretinin, J. Park, L. A. Ponomarenko, M. I. Katsnelson, Y. N. Gornostyrev, K. Watanabe, T. Taniguchi, C. Casiraghi, H.-J. Gao, A. K. Geim, and K. S. Novoselov, Nat. Phys. **10**, 451 (2014).
[44] T. Stauber, N. M. R. Peres, and A. K. Geim, Phys. Rev. B **78**, 085432 (2008).
[45] F. Hipolito and V. M. Pereira, 2D Mater. **4**, 021027 (2017).